

The influence of inertia and contact angle on the instability of partially wetting liquid strips. A numerical analysis study

Sebastián Ubal,^{1, a)} Paul Grassia,^{2, b)} Diego M. Campana,^{1, c)} María D. Giavedoni,^{1, d)}
and Fernando A. Saita^{1, e)}

¹⁾*Instituto de Desarrollo Tecnológico para la Industria Química,
UNL-CONICET, Güemes 3450, 3000, Santa Fe (capital),
Argentina*

²⁾*CEAS, The Mill, The University of Manchester, Oxford Road, Manchester,
M13 9PL, United Kingdom*

(Dated: 23 January 2014)

The stability of a thread of fluid deposited on a flat solid substrate is studied numerically by means of the Finite Element Method in combination with an Arbitrary Lagrangian-Eulerian technique. A good agreement is observed when our results are compared with predictions of linear stability analysis obtained by other authors. Moreover, we also analysed the influence of inertia for different contact angles and found that inertia strongly affects the growth rate of the instability when contact angles are large. By contrast, the wavenumber of the fastest growing mode does not show important variations with inertia. The numerical technique allows us to follow the evolution of the free surface instability until comparatively late stages, where the filament begins to break into droplets. The rupture pattern observed for several cases shows that the number of principal droplets agrees reasonably well with an estimation based on the fastest growing modes.

^{a)}subal@santafe-conicet.gov.ar (corresponding author); Also at Facultad de Ingeniería, UNER, Ruta Prov. No. 11, KM 10, 3101, Oro Verde, Entre Ríos, Argentina

^{b)}paul.s.grassia@manchester.ac.uk

^{c)}dcampana@santafe-conicet.gov.ar; Also at Facultad de Ingeniería, UNER, Ruta Prov. No. 11, KM 10, 3101, Oro Verde, Entre Ríos, Argentina

^{d)}madelia@santafe-conicet.gov.ar

^{e)}fasaita@santafe-conicet.gov.ar

I. INTRODUCTION

Free surface flow instabilities have been, and are, the subject of very active research. The presence of contact lines introduces an additional difficulty in the analysis of these phenomena. This paper addresses in particular the instability of a slender strip of fluid that is deposited on a flat solid surface. Liquid ribbons like these can be seen in everyday life, as on car windscreens or in breaking uniform fluid films. Their study is also important in applications like *Direct-Write*¹⁻⁴, printed electronics⁵ and material functionalisation⁶, which are different kinds of micro- and nano-fluidics applications⁷. The knowledge of the stability properties of this system is of fundamental importance, either because the breakup into droplets is an unwanted phenomenon or because a regular rupture pattern is desired. It is also a scientifically interesting problem in its own right.

The pioneering work of Davis⁸, based on a kinetic energy balance, reveals that fluid rivulets with fixed contact lines are stable if $\theta < \pi/2$ (θ being the contact angle), while if $\theta > \pi/2$ only perturbations of a wave number (k) larger than a critical value (k_C) are stable. Moreover, when the contact line is free to move and θ is a smooth function of the contact line speed, Davis showed that there always exists a critical wave number above which perturbations are stable.

Subsequent works have found that the existence of axial flows^{9,10} and the influence of gravity^{11,12} both have a stabilising effect. The stability of liquid threads deposited in V-shaped substrates was studied by Langbein¹³, Roy and Schwartz¹⁴, Yang and Homsy¹⁵. The paper by Diez, González, and Kondic¹² provides a detailed account of linear stability analyses carried out in previous works. They also derived a lubrication based equation for the evolution of the film thickness, which accounts for the gravity forces and the liquid-solid interaction effects through the disjoining pressure. In this sense, the model can be used to simulate both macroscopic and microscopic fluid rivulets. In addition to a linear stability analysis of this new model, they also conducted numerical simulations of infinite and finite fluid strips by solving a lubrication-based evolution equation. For infinite strips, these authors found that the wavelength with maximum growth rate predicted by the linear stability analysis coincides with the distance between droplets resulting from the non-linear simulations. Similar conclusions hold for finite strips, at least in the explored range of parameters.

Experimental studies of the problem were presented by Schiaffino and Sonin¹⁶, Duineveld¹⁷, González *et al.*¹⁸ and Kondic *et al.*⁶. Schiaffino and Sonin¹⁶ worked with strips of molten wax deposited in a cool substrate to freeze the contact line, finding a reasonable agreement with Davis’s theory. Kondic *et al.*⁶ analysed the stability of nano-strips of nickel by using a pulsed laser to melt the metal. They found that the time and length scales measured in the experiments agree reasonably well with predictions of an isothermal hydrodynamic model. The experiments also show that, for thin lines, finite size effects produced at the ends of the filament are weak and the instability progresses almost uniformly along its length; by contrast, for thicker strips border effects have stronger influence on the evolution. These observations are consistent with those of González *et al.*¹⁸, who studied the instability of 0.3–1 mm thick and 5 cm long strips under partially wetting conditions and observed that the instability always starts at the ends of the filament and progress toward its central region.

This paper focuses on one aspect of the problem not explored until now: the influence of inertia on the stability of the system, particularly for large contact angles. In spite of the small cross section of the filaments that are relevant to, say, printed electronics applications, the use of fluids of particularly low viscosity or/and large density raise the question of whether or not it is a valid approximation to ignore this effect. We also compare our results with those from previous works. Our model considers a fragment of a Newtonian liquid thread, whose shape repeats periodically on both sides of the modelled segment. Physico-chemical properties are assumed constant, as well as the dynamic contact angle (which equals the static one). The contact line singularity is relieved by a Navier’s slip condition¹⁹. The governing equations are solved numerically by the Finite Element Method, combined with an Arbitrary Lagrangian-Eulerian technique²⁰, that allows us to follow the time evolution of the liquid thread after an initial perturbation until late stages of the evolution, where the filament breaks into droplets.

II. PHYSICAL MODEL

A filament of a Newtonian fluid with constant properties (density ρ , viscosity μ and surface tension σ) rests on a flat solid surface (see Fig. 1). The surrounding air is calm and regarded as inviscid; its constant pressure is taken as the reference pressure of the system

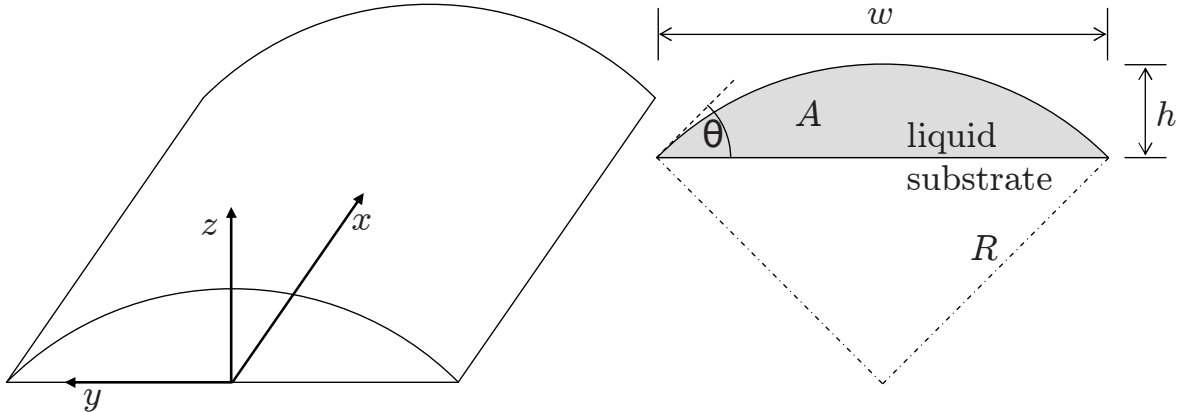


FIG. 1. Sketch of the domain, the coordinate system and some geometric definitions.

and arbitrarily set to zero. In an undisturbed state, the rivulet cross section area (A) is constant, and the contact angle at the triple line solid–liquid–gas is θ , assumed also constant. We define R as the curvature radius that the rivulet should have in a static configuration in the absence of gravity effects

$$A = R^2 \left(\theta - \frac{\sin 2\theta}{2} \right). \quad (1)$$

In order to study the stability of the thread of fluid, we impose an axial sinusoidal perturbation to its radius, whose amplitude is B and wave number is k , but taking into consideration that the volume of the original strip of fluid is preserved. We analyse the time evolution on a fragment of the rivulet of length π/k , i.e. half a wavelength of the initial perturbation. The motion of the liquid is governed by the equations of Navier-Stokes and continuity

$$\rho \left(\frac{\partial \mathbf{v}}{\partial t} + \mathbf{v} \cdot \nabla \mathbf{v} \right) = -\nabla p + \nabla \cdot \boldsymbol{\tau} + \rho \mathbf{g}, \quad (2)$$

$$\nabla \cdot \mathbf{v} = 0, \quad (3)$$

$\boldsymbol{\tau} = 2\mu \mathbf{D}$ being the viscous part of the stress tensor (\mathbf{T}), $\mathbf{D} = 1/2 \left[\nabla \mathbf{v} + (\nabla \mathbf{v})^T \right]$ the strain rate tensor and $\mathbf{g} = -g \mathbf{e}_z$ the acceleration of gravity.

The liquid–air interface is a material surface, therefore the following kinematic condition applies

$$(\mathbf{v} - \dot{\mathbf{x}}_{\text{FS}}) \cdot \mathbf{n} = 0, \quad (4)$$

\mathbf{n} being the external unit normal vector and $\dot{\mathbf{x}}_{\text{FS}}$ the velocity of the free surface. Surface

tension exerts a normal stress at the liquid–air interface

$$\mathbf{n} \cdot \mathbf{T} = \sigma \kappa \mathbf{n}, \quad (5)$$

$\kappa = -\nabla_S \cdot \mathbf{n}$ being the curvature of the free surface, $\nabla_S = \mathbf{I}_S \cdot \nabla$ the surface gradient operator and $\mathbf{I}_S = \mathbf{I} - \mathbf{n}\mathbf{n}$ the surface identity tensor.

At both ends of the liquid thread ($x = 0$ and $x = \pi/k$) symmetry conditions are applied, both for the velocity field and the shape of the free surface.

On the liquid–solid interface, the no-slip condition ($\mathbf{v} = \mathbf{0}$) is applied, except on a narrow region close to the moving contact line. On this narrow region, a Navier’s slip condition²¹ is employed to relieve the stress singularity at the contact line¹⁹

$$\mathbf{n} \cdot \mathbf{T} \cdot \mathbf{t} = -\frac{\mu}{L_S} \mathbf{t} \cdot \mathbf{v}, \quad (6)$$

where \mathbf{t} is *any* unit vector tangent to the solid–liquid interface and L_S is the slip-length, a phenomenological parameter that can be interpreted as the distance down into the substrate at which the extrapolated velocity profile becomes zero. Besides, since the solid substrate is impermeable, the normal component of the velocity is zero, $\mathbf{v} \cdot \mathbf{e}_z = 0$.

At the moving contact line, the contact angle (θ) needs to be prescribed.

$$\boldsymbol{\mu} \cdot \mathbf{e}_z = -\sin \theta, \quad (7)$$

$\boldsymbol{\mu}$ being a unit vector normal to the contact line and tangent to the free surface.

We proceed now to make the stated problem dimensionless. Lengths are scaled with R , velocities with σ/μ , time with $R\mu/\sigma$ and stresses with σ/R . The dimensionless versions of eqs. 1, 2, 5 and 6 are

$$\hat{A} = \frac{A}{R^2} = \theta - \frac{\sin 2\theta}{2}, \quad (8)$$

$$La \left(\frac{\partial \hat{\mathbf{v}}}{\partial \hat{t}} + \hat{\mathbf{v}} \cdot \hat{\nabla} \hat{\mathbf{v}} \right) = -\hat{\nabla} \hat{p} + \hat{\nabla} \cdot \hat{\boldsymbol{\tau}} - Bo \mathbf{e}_z, \quad (9)$$

$$\mathbf{n} \cdot \hat{\mathbf{T}} = \hat{\kappa} \mathbf{n}, \quad (10)$$

and

$$\mathbf{n} \cdot \hat{\mathbf{T}} \cdot \mathbf{t} = -\frac{1}{\mathcal{L}} \mathbf{t} \cdot \hat{\mathbf{v}}, \quad (11)$$

where $La = \rho\sigma R/\mu^2$ is the Laplace number, $Bo = \rho g R^2/\sigma$ is the Bond number and $\mathcal{L} = L_S/R$ is the dimensionless slip-length. Equations 3 and 4 read the same, but replacing operators and variables by their dimensionless counterparts. Notice that the dimensionless extent of the domain along the \hat{x} -axis is π/\hat{k} .

In the next section we explain briefly the numerical technique employed to solve the governing equations stated above.

III. NUMERICAL METHOD

The equations modelling the time evolution of the liquid thread, eqs. 9 and 3, along with the boundary conditions stated in the previous section, were solved numerically by the Finite Element Method (FEM). Notice that the domain where equations are solved is *a priori* unknown and changes with time. There are several numerical techniques aimed at tackling free boundary problems like this, traditionally clasified as “interface capturing” [e.g. Volume of Fluid^{22,23}, Level-Set^{24,25} and Diffuse-Interface^{26,27}] and “interface tracking” [e.g. Lagrangian^{28,29} and Arbitrary Lagrangian-Eulerian^{30–33} techniques] methods.

In this paper we employ an Arbitrary Lagrangian Eulerian (ALE) formulation embedded in the FEM software COMSOL Multiphysics³⁴. In ALE techniques (and in Lagrangian techniques as well) the numerical mesh follows and adapts to the distorting domain (the liquid rivulet in our case), but grid points do not necessarily follow material points. In particular, we use the so-termed “Winslow smoothing method”³⁵, which specifies that the initial position, $\hat{\mathbf{X}}(\hat{\mathbf{x}}, \hat{t})$, of mesh points currently situated at $\hat{\mathbf{x}}$, is governed by the equation

$$\hat{\nabla}^2 \hat{\mathbf{X}} = 0. \tag{12}$$

The boundary conditions at the free surface for eq. 12 are obtained from the application of the Lagrange multipliers technique³⁶ to eq. 4. The remaining boundary conditions are zero normal derivatives ($\partial \hat{\mathbf{X}}/\partial n = \mathbf{n} \cdot \hat{\nabla} \hat{\mathbf{X}} = 0$) except where essential boundary conditions apply (at the solid substrate $\hat{Z} = \hat{z} = 0$, at the **symmetry planes** $\hat{X} = \hat{x} = 0$ and $\hat{X} = \hat{x} = \pi/\hat{k}$).

COMSOL solves eqs. 9, 3 and 12 along with their boundary conditions by means of the Galerkin/FEM. The domain is discretised in an unstructured mesh of tetrahedra. Velocities and space coordinates are approximated by quadratic Lagrangian basis functions, while pressure is interpolated by linear Lagrangian basis functions. A variable order, totally

implicit, finite difference scheme is employed for time discretisation. Newton iteration is used to solve the resulting set of non-linear algebraic equations. A more detailed description of the numerical technique and its validation can be found in Ubal *et al.*³⁷, where the authors study the deposition of a line of fluid on a plane substrate, rather than the stability of an already deposited filament, as is the case in this work.

A. The setting up of the numerical experiments

As mentioned in previous sections, the aim of this work is to study the stability of a thread of fluid deposited on a flat solid substrate by direct numerical simulation. Each numerical experiment starts with the fluid at rest, with the shape of the fluid strip possessing an initial sinusoidal perturbation to its radius, the perturbation wavelength being $2\pi/\hat{k}$ and its amplitude being \hat{B} . In this work we have employed a value of $\hat{B} = 0.01$. From this initial condition, the simulation evolves in time, and two different behaviours develop, depending on the set of parameters employed: a stable time evolution, or an unstable one. In the first case, the perturbation decays and finally a straight rivulet is observed. In the second case, the perturbation grows and the free surface evolves towards a rupture pattern.

The main parameters of the problem are θ (or equivalently \hat{A}), La , Bo and \hat{k} . In addition, there are other parameters that need to be specified, including the mesh size, the width of the region (on the substrate, adjacent to the contact line) where the slip condition applies, and the value of the slip-length (\mathcal{L}). The simulations presented in this paper were carried out for $\mathcal{L} = 0.05$, a width for the slip region equal to 5% of the strip local width (which changes in time) and a mesh whose elements, at $\hat{t} = 0$, vary from a minimum size of 0.05 (near the contact line) to a maximum size of 0.8 (near the apex of the filament, for those cases with a large θ). We carried out several tests aimed to study the sensitivity of the results to these parameters. For $\theta = \pi/6$, $La = 4.11$, $Bo = 0.132$ and $\hat{k} = 1.2$ we observed that the linear growth rate (α , see definition in eq. (13)): (a) varies less than 5% when \mathcal{L} changes from 0.005 to 0.5, for a slip region of 5% of the local strip width; (b) varies less than 10% when the slip region changes from 1% to 10% of the local strip width, for $\mathcal{L} = 0.05$. We also observed that the critical wave number determined (\hat{k}_C) is insensitive to either of these parameters. Independence of the results on the mesh size was verified as well. Finally, we successfully compared our numerical results against theoretical predictions from other

authors, as will be seen in sec. IV A.

IV. RESULTS

A. Comparison with previous works

In order to assess the validity and capabilities of our model, we carried out a series of simulations aimed to compare our results with those from other authors.

Figure 2 shows the critical (marginal) wave numbers (scaled with the square root of the cross section area, $\hat{k}_C \hat{A}^{1/2}$) as a function of the contact angle (θ). The solid curve corresponds to the predictions of Davis⁸ while the symbols to our numerical results: *crosses* indicate numerical experiments whose time evolution were *unstable*, while *circles* correspond to simulations with a *stable* outcome. In the paper by Davis⁸ gravity is neglected, and inertia is not relevant in the determination of \hat{k}_C . Our model however includes these effects: we set $La\hat{A}^{1/2} = 1.24$ and $Bo\hat{A} = 0.012$, i.e. inertia and gravity effects are both kept small. This combination of parameters corresponds to the fact that our numerical experiments were carried out for strips with a fixed (dimensional) cross section area. If we adopt the following values of density ($\rho = 1000 \text{ kg m}^{-3}$), surface tension ($\sigma = 0.05 \text{ N m}^{-1}$), viscosity ($\mu = 0.1 \text{ Pa s}$) and gravity acceleration ($g = 9.8 \text{ m s}^{-2}$), the resulting cross section area is $A = 6.1 \times 10^{-8} \text{ m}^2$. Note however that in order to keep A constant, the (dimensional) curvature radius of the unperturbed thread of liquid diminishes as the contact angle θ increases from 0 to π .

Figure 2 shows that our stable/unstable results are correctly situated above/below the prediction of Davis. However, the “resolution” in $\hat{k}\hat{A}^{1/2}$ employed (minimum difference between wave numbers tested) in our simulations was poorer for larger θ .

We also evaluated the growth rate (α) of the disturbance applied to the strip shape, at early stages of the time evolution. To this end, we **performed a Discrete Fourier Transform of the shape of the strip width, that can be written as follows**

$$\hat{w}(\hat{x}, \hat{t}) \approx \hat{w}_0(\hat{t}) + \hat{w}_1(\hat{t}) \exp(i\hat{k}\hat{x}) + \hat{w}_2(\hat{t}) \exp(i2\hat{k}\hat{x}) + \dots, \quad (13)$$

where the time varying amplitudes ($\hat{w}_n(\hat{t})$, $n = 1, 2, \dots$) of the spatial modes are approxi-

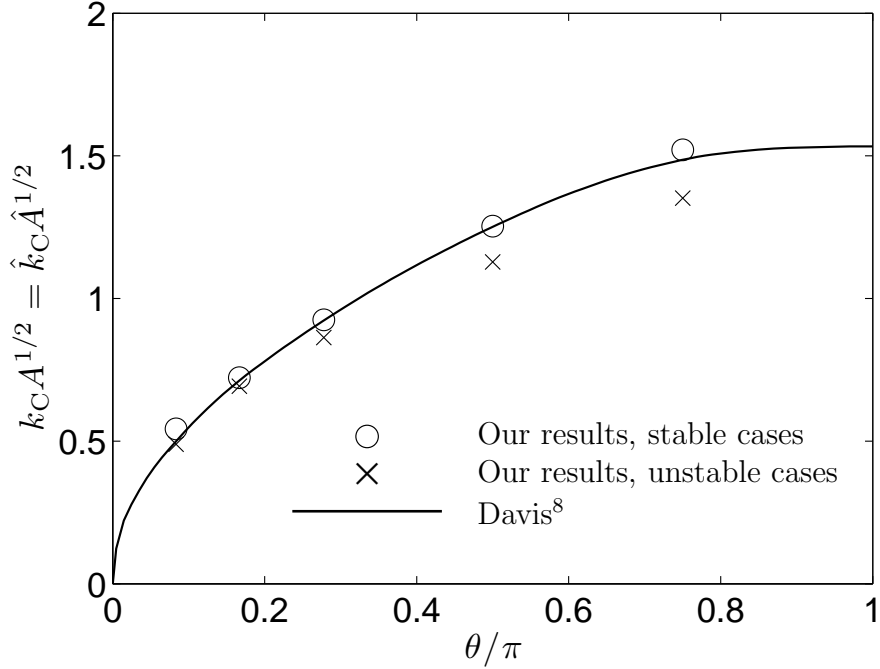


FIG. 2. Critical wave numbers (scaled with the square root of the cross section area) as a function of the contact angle. Our results were computed for $La\hat{A}^{1/2} = 1.24$ and $Bo\hat{A} = 0.012$.

mately given at early times by

$$\begin{aligned}
 \hat{w}_1(\hat{t}) &\approx \hat{w}_1^0(\hat{t}) + c_1 \exp(\alpha\hat{t}), \\
 \hat{w}_2(\hat{t}) &\approx \hat{w}_2^0(\hat{t}) + c_2 \exp(\beta\hat{t}), \\
 &\vdots
 \end{aligned}
 \tag{14}$$

We then extracted α from the analysis of the time evolution of $\hat{w}_1(\hat{t})$ in eq. (14). The terms $\hat{w}_n^0(\hat{t})$ are rapidly decaying transients, that are produced due to the initial condition employed, before the exponential growth regime dominates the time evolution.

As an example, Fig. 3 shows the dispersion relationship (α as a function of \hat{k}) for $\theta = 5\pi/18$ ($\hat{A} = 0.380$), $La = 2.01$ and $Bo = 0.0316$ (note that we keep the same values of $La\hat{A}^{1/2} = 1.24$ and $Bo\hat{A} = 0.012$). The solid curve represents the results from Diez, González, and Kondic¹² [see the solid curve for $\tilde{p} = 5$ (or $\tilde{A} \equiv Bo\hat{A} = 0.012$) in Fig. 9 of that paper]. The circles are our results. As can be seen, the agreement is very good, except for the largest negative growth rate (stable case). In particular, the maximum growth rate and the critical wave number (\hat{k}_C , the zero-crossing wave number) are both reproduced well.

Finally, we also compared our results with those from Diez, González, and Kondic¹² and

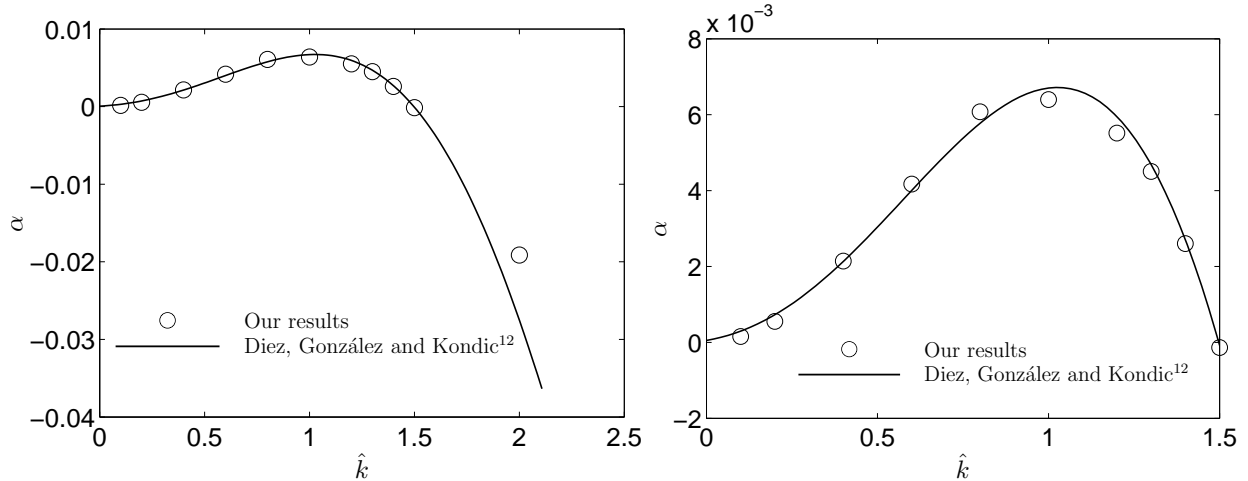


FIG. 3. Dispersion relationship (linear growth rate versus wave number) for $\theta = 5\pi/18$ ($\hat{A} = 0.380$) and $Bo = 0.0316$. Our results were computed for $La = 2.01$.

Sekimoto, Oguma, and Kawasaki¹¹ for non-negligible gravity effects. We fixed the values of $\theta = \pi/6$ ($\hat{A} = 0.0906$) and $La = 4.11$ (again, we maintain the value of $La\hat{A}^{1/2} = 1.24$), and varied Bo . The comparison is displayed in Fig. 4. The solid curve is the prediction by Diez, González, and Kondic¹², the dashed curve the results from Sekimoto, Oguma, and Kawasaki¹¹ and the symbols our results, with the same convention as in Fig. 2. These results seem to indicate that our numerical results are closer to those of Diez, González, and Kondic¹², while the predicted \hat{k}_C of Sekimoto, Oguma, and Kawasaki¹¹ are slightly larger over almost the whole range of Bo depicted.

In the next section we study the influence of inertia for different contact angles.

B. Inertia effects for different contact angles

In this section we explore the effect of inertia on the time evolution of liquid threads forming different contact angles with the substrate, after their cross section area is perturbed. Let us recall that we have already computed critical wave numbers for different contact angles (including values equal and above $\pi/2$) in sec. IV A: it is important to point out that inertia does not affect the values of \hat{k}_C . The results presented below were obtained for $Bo\hat{A} = 0.012$. For fixed values of density ($\rho = 1000 \text{ kg m}^{-3}$), surface tension ($\sigma = 0.05 \text{ N m}^{-1}$) and gravity acceleration ($g = 9.8 \text{ m s}^{-2}$), this means that fluid lines have constant cross section area ($A = 6.1 \times 10^{-8} \text{ m}^2$).

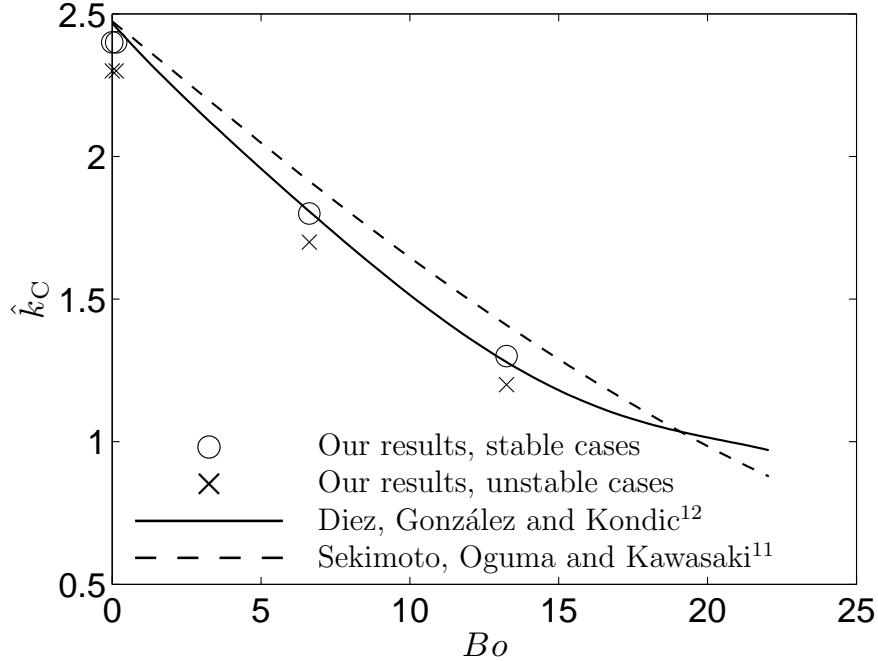


FIG. 4. Critical wave numbers as a function of the Bond number, for $\theta = \pi/6$ ($\hat{A} = 0.0906$). Our results were computed for $La = 4.11$.

1. Results for early times of the evolution

We first restrict our analysis to the early times of the evolution of the process, paying particular attention to the linear (exponential) growth rates (α). Figure 5 shows the dispersion relationship (α as a function of \hat{k}) for $\theta = \pi/6$ ($\hat{A} = 0.0906$), for $La\hat{A}^{1/2} = 1.24$ ($\mu = 0.1$ Pa s, squares and dashed curve), $La\hat{A}^{1/2} = 1.24 \times 10^2$ ($\mu = 0.01$ Pa s, triangles and dot-dashed curve) and $La\hat{A}^{1/2} = 1.24 \times 10^4$ ($\mu = 0.001$ Pa s, circles and solid curve). The symbols represent the actual outcome from the numerical simulations (and their subsequent post-processing), while the curves are polynomial fits of 5th order of these data. We adopted polynomials of the form $\alpha = \hat{k}^2(b_0 + b_1\hat{k} + b_2\hat{k}^2 + b_3\hat{k}^3)$ because, on one hand, $\alpha \rightarrow 0$ as $\hat{k} \rightarrow 0$ owing to volume conservation and, on the other hand, the asymptotic behaviour of α for small \hat{k} obtained by Yang and Homsy¹⁵ and Brochard-Wyart and Redon³⁸ is of the form $\alpha \sim C\hat{k}^2$, with C a constant.

Figure 5 clearly shows that the influence of inertia is moderate: growth rates seem to first increase slightly and then decrease noticeably. α diminishes by roughly a 20% from the smallest to the largest La computed, while \hat{k}_M increases slightly.

We obtained similar results for $\theta = \pi/2$ ($\hat{A} = \pi/2$) and the same values of $La\hat{A}^{1/2}$; these

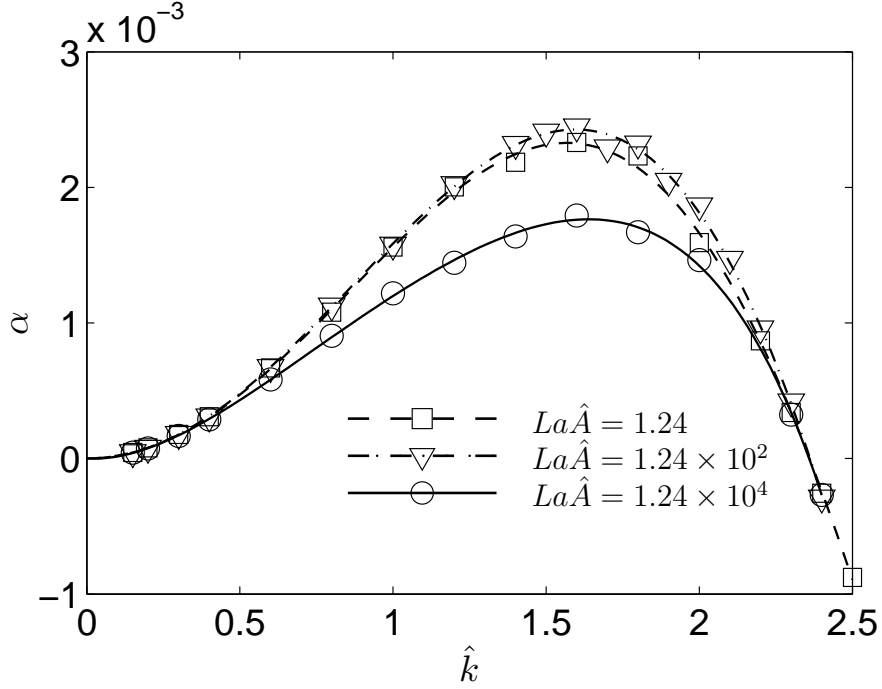


FIG. 5. The influence of inertia on the dispersion relationship (linear growth rate versus wave number) for $\theta = \pi/6$ ($\hat{A} = 0.0906$) and $Bo\hat{A} = 0.012$. Symbols are the actual values of α computed numerically; curves represent 5th order polynomial fits of these data.

are displayed in Fig. 6. Now the influence of inertia is more important. Compared to the case for $La\hat{A}^{1/2} = 1.24$, the values of α reduce to 75% and 17% of the reference value, as La increases in steps of a hundredfold. As before, the influence of inertia on \hat{k}_M is only weak.

Finally, we also computed the dispersion relationship for $\theta = 3\pi/4$ ($\hat{A} = 2.86$) and the same values of $La\hat{A}^{1/2}$. Results are depicted in Fig. 7. In this case the influence of inertia on the maximum growth rate is very important: the value of α computed for the viscous case ($La\hat{A}^{1/2} = 1.24$) is about twice and 14 times larger than the values obtained when La increases by 100 and 10^4 , respectively. Again, the value of \hat{k}_M undergoes a small increment as inertia becomes important.

For the results above described, it is important to remark that α is a non-dimensional growth rate. Since the characteristic time is $\mu R/\sigma$, even though dimensionless growth rates reduce with La , dimensional ones increase owing to the decrease in viscosity (and characteristic time $\mu R/\sigma$, which divides α to produce the dimensional growth rate).

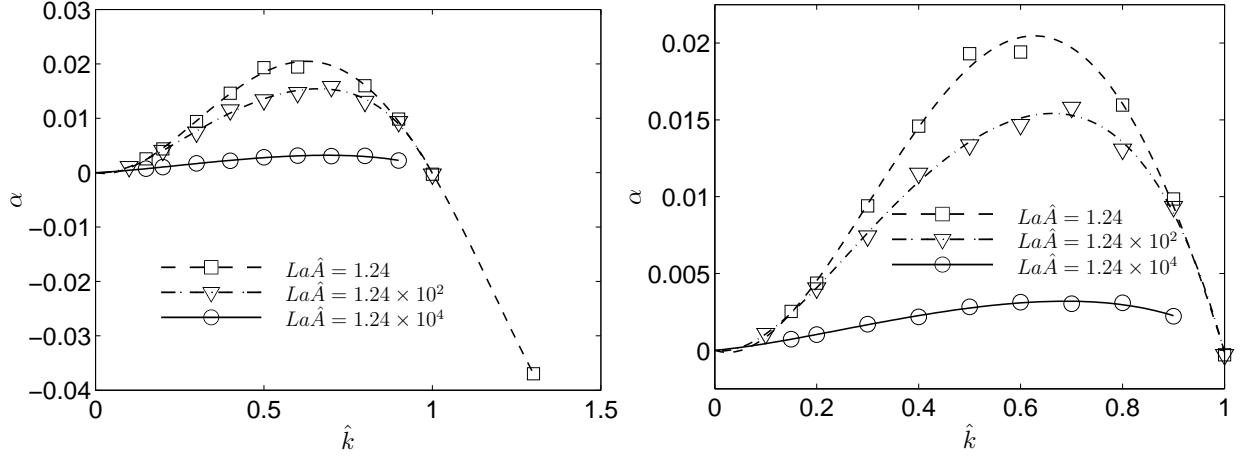


FIG. 6. The influence of inertia on the dispersion relationship (linear growth rate versus wave number) for $\theta = \pi/2$ ($\hat{A} = \pi/2$) and $Bo\hat{A} = 0.012$. Symbols are the actual values of α computed numerically; curves represent 5th order polynomial fits of these data. The graph on the right shows the same data as the graph on the left, over a restricted range of \hat{k} and α .

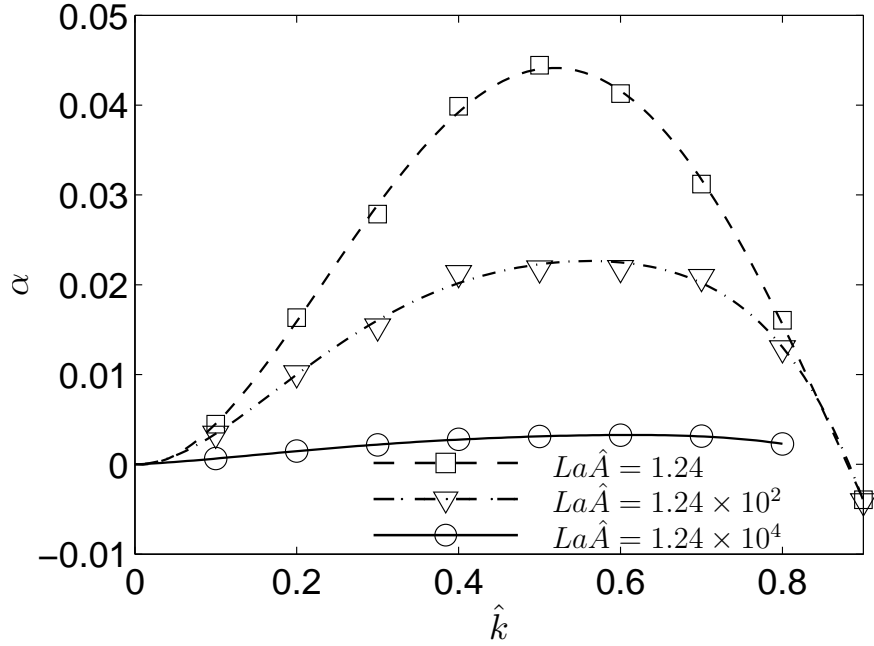


FIG. 7. The influence of inertia on the dispersion relationship (linear growth rate versus wave number) for $\theta = 3\pi/4$ ($\hat{A} = 2.86$) and $Bo\hat{A} = 0.012$. Symbols are the actual values of α computed numerically; curves represent 5th order polynomial fits of these data.

2. The evolution of the liquid thread for long times

In previous sections the focus was in the behaviour of the liquid thread at early times of the evolution, when the perturbation of the cross section area either starts to grow ($\hat{k} < \hat{k}_C$) or decays towards a uniform value ($\hat{k} > \hat{k}_C$). Since unstable wave numbers grow at varying rates—and a fastest growing mode (let us define \hat{k}_M as the wave number of this mode) can be identified—it is worth analysing the development of the instability at long times and observe the competition of different modes, when either viscous or inertial effects are dominant. To this end, we study the time evolution of four of the unstable cases already computed in previous sections: (a) $\theta = \pi/6$ ($\hat{A} = 0.0906$), $La\hat{A}^{1/2} = 1.24$ and $\hat{k} = 0.15$, (b) $\theta = \pi/6$, $La\hat{A}^{1/2} = 1.24 \times 10^4$ and $\hat{k} = 0.15$, (c) $\theta = 3\pi/4$ ($\hat{A} = 2.86$), $La\hat{A}^{1/2} = 1.24$ and $\hat{k} = 0.1$, and (d) $\theta = 3\pi/4$, $La\hat{A}^{1/2} = 1.24 \times 10^4$ and $\hat{k} = 0.1$. As can be noticed, we chose perturbations with wavelengths several times longer than the fastest growing modes.

Besides, as stated at the beginning of sec. IV B, in all the cases $Bo\hat{A} = 0.012$, which can be interpreted as keeping constant the (dimensional) cross section ($A = 6.1 \times 10^{-8} \text{ m}^2$) if, in addition, we adopt the following fixed values of density ($\rho = 1000 \text{ kg m}^{-3}$), surface tension ($\sigma = 0.05 \text{ N m}^{-1}$) and gravity acceleration ($g = 9.8 \text{ m s}^{-2}$).

Figures 8–11 show the results corresponding to cases (a)–(d) above. Each frame depicts the shape of the liquid strip for a given instant of time. Shadings (colours in online version) illustrate the value of the pressure.

Case (a) (Fig. 8) shows the development of the instability, starting from the initial perturbation (the domain comprises half a wavelength) to the final state that can be attained with our numerical technique, where one of the necks ($\hat{x} \sim 10$) has practically undergone a pinch-off process. Note that the ALE-based scheme we employ does not support changes in the domain topology. Therefore, if one of the (assuming multiple) necks reaches the pinch-off before others, the process occurring after that point in time can not be observed with the present technique. At $\hat{t} = 2069$, a number of narrowings appear at $\hat{x} \sim 7, 11$ and 17 (there is another at $\hat{x} \sim 20$ originated by the initial condition) where, moreover, the pressure is locally higher owing to the larger curvature of the free surface. As time advances ($\hat{t} = 2852$) these regions continue thinning and some new appear at $\hat{x} \sim 3$ and 14 . The final pattern attained with our scheme ($\hat{t} = 3269$) suggest the the instability process would end up with about 11 large droplets and at least 3 smaller droplets in a whole wavelength (considering

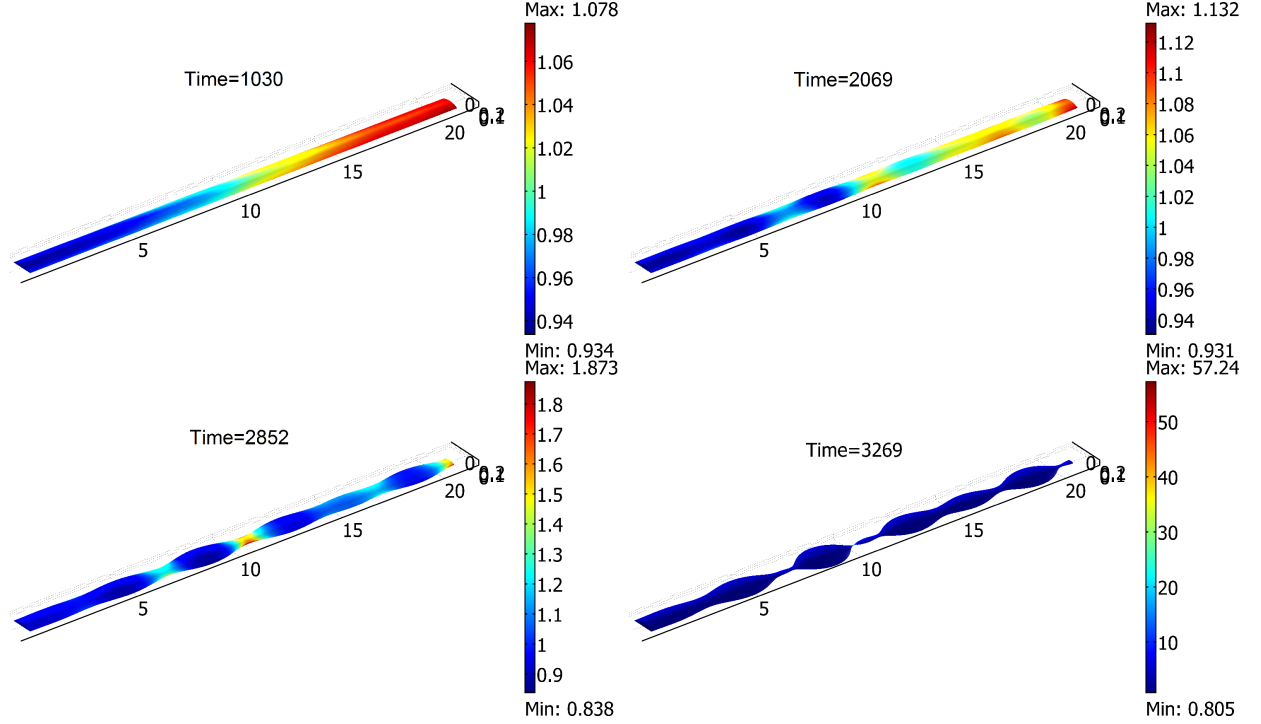


FIG. 8. (Colour online) The time evolution of a liquid strip with an initial perturbation of wave number $\hat{k} = 0.15$. The remaining parameters are $\theta = \pi/6$ ($\hat{A} = 0.0906$), $Bo\hat{A} = 0.012$ and $La\hat{A}^{1/2} = 1.24$. Shadings (colours in online version) indicate values of pressure (scale on the right of each frame). Instants of dimensionless time are printed for reference. The corresponding dimensional times (considering $R = 8.22 \times 10^{-4}$ m, $\sigma = 0.05$ N m $^{-1}$ and $\mu = 0.1$ Pas) are 1.69 s, 3.40 s, 4.69 s and 5.37 s.

the symmetry of our simulated system, where only a half wavelength is shown). A rough calculation (\hat{k}_M/\hat{k}) predicts the formation of about 10–11 droplets of the fastest growing mode, which compares reasonably well with the computations.

When viscosity is decreased (case (b), Fig. 9) and the contact angle is kept small, the instability process observed is practically the same, except for the time scale. In terms of dimensionless time, the first pinch-off ($\hat{x} \sim 10$) is produced somewhat (1.4 times) later than in case (a). However (and recalling that times are made non-dimensional with $R\mu/\sigma$) if one considers that the only change in going from case (a) to (b) is a hundredfold decrease in viscosity, a simple calculation shows that actually attaining pinch-off in case (b) takes $\sim 1.4\%$ of the time that it takes in case (a).

Let us now consider increasing the contact angle, compared to case (a), but maintaining

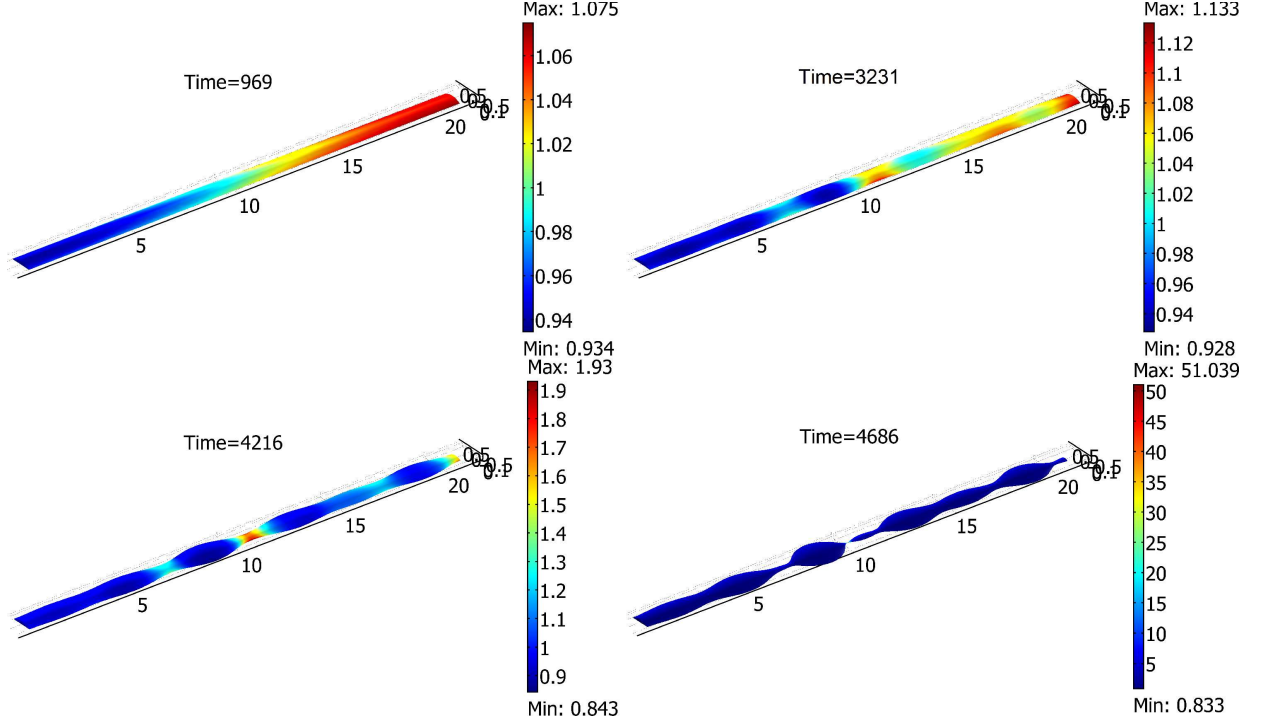


FIG. 9. (Colour online) The time evolution of a liquid strip with an initial perturbation of wave number $\hat{k} = 0.15$. The remaining parameters are $\theta = \pi/6$ ($\hat{A} = 0.0906$), $Bo\hat{A} = 0.012$ and $La\hat{A}^{1/2} = 1.24 \times 10^4$. Shadings (colours in online version) indicate values of pressure (scale on the right of each frame). Instants of dimensionless time are printed for reference. The corresponding dimensional times (considering $R = 8.22 \times 10^{-4}$ m, $\sigma = 0.05$ N m $^{-1}$ and $\mu = 0.001$ Pa s) are 0.0159 s, 0.0531 s, 0.0693 s and 0.0770 s.

the same (dimensional) cross section area (case (c), Fig. 10). To accomplish this, the (dimensional) radius of the straight liquid filament (R) is made ~ 5.6 times smaller. After the initial condition ($\hat{t} = 149.3$), the liquid thread evolves producing two narrowings at $\hat{x} \sim 7$ and 19, besides the original one at $\hat{x} \sim 30$. These regions continue thinning ($\hat{t} = 170.3$ and 185.4) but at some point ($\hat{t} = 204.0$) these long necks give rise to the formation of small bulges limited in turn by smaller constrictions. When the first pinch-off ($\hat{x} \sim 14$) is practically attained ($\hat{t} = 206.6$), the final pattern observed suggest the formation of 5 large droplets along with other 5 smaller droplets³⁹, in a complete wavelength. The same rough estimate as before predicts the formation of about 5 droplets of the fastest growing mode. In dimensionless terms, the time elapsed until the first pinch-off is a 6.3% of the time demanded in case (a). When the decrease in R is accounted, one obtains that reaching the

pinch-off actually takes considerably less (dimensional) time: 1.1% of that in case (a). Either in dimensionless or in dimensional terms, it is remarkable the acceleration of the break-up process observed when θ is increased.

Finally, let us take case (c) as a base for comparison, and reduce the viscosity 100 times (case (d), Fig. 11). As can be observed, in this case inertia has important effects on the pattern of break up displayed by the liquid filament. During the early stages (up to $\hat{t} = 2294$) of the instability, one can observe the formation of necks about the same locations as in case (c). It is however in late stages when differences appear. When inertia is important compared to viscous forces, the constrictions **that —as a result of the instability process— become more pronounced than others evolve faster** and, as a consequence, those locations attain the pinch off before the other necks. This contrasts the behaviour observed in case (c) (Fig. 10), where the break up of the filament seems to be attained more or less at the same time in all the narrowings. For this reason, it is difficult to establish the final pattern of break up in case (d). One can speculate that the evolution would end up with about 5 large droplets and possibly 3 smaller droplets within a distance of one wavelength, but simulations for longer times are required to ascertain to this point. According to the calculations shown in section IV B 1, one could estimate the formation of about 6 droplets, based on the wave number of the fastest growing mode. We can also observe that the (dimensionless) time elapsed to attain the first break up is ~ 13 times that corresponding to the viscous case (c). Recalling the comparison of pinch-off times of cases (a) and (b), we can infer that the effect of the inertial term in eq. (9) is more important for large contact angles (θ) and **hence large** dimensionless cross **sectional** areas (\hat{A}). However, as before, considering that the only change in going from case (c) to (d) is a hundredfold decrease in viscosity, it turns out that, in fact, the dimensional time for filament rupture in case (d) is $\sim 13\%$ of that of case (c). Indeed the dimensional times indicated in Figure 11 are very short, implying (for practical experimental purposes) a near instantaneous break up of a filament as it is being laid down (as opposed to an instability on an already deposited filament).

V. DISCUSSION AND CONCLUSIONS

In this paper we analyse the capillary instability process undergone by a segment of fluid rivulet deposited on a flat solid substrate, with symmetry conditions at both ends

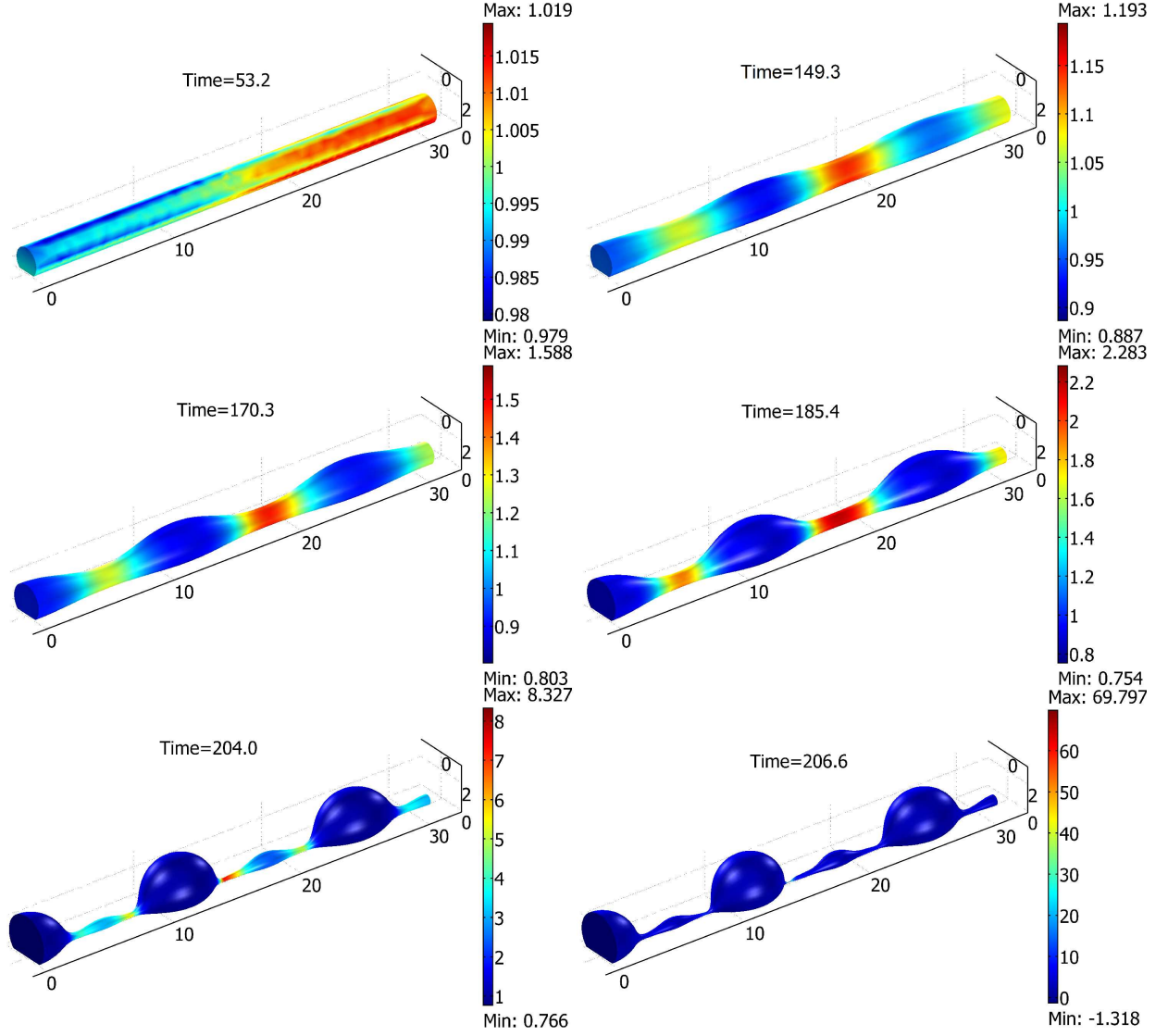


FIG. 10. (Colour online) The time evolution of a liquid strip with an initial perturbation of wave number $\hat{k} = 0.1$. The remaining parameters are $\theta = 3\pi/4$ ($\hat{A} = 2.86$), $Bo\hat{A} = 0.012$ and $La\hat{A}^{1/2} = 1.24$. Shadings (colours in online version) indicate values of pressure (scale on the right of each frame). Instants of dimensionless time are printed for reference. The corresponding dimensional times (considering $R = 1.46 \times 10^{-4}$ m, $\sigma = 0.05$ N m $^{-1}$ and $\mu = 0.1$ Pa s) are 0.0156 s, 0.0437 s, 0.0499 s, 0.0543 s, 0.0597 s and 0.0605 s. **The noisy variations in shading (colour in online version) visible for $t = 53.2$ are partly due to a lightning effect in the picture and partly due to small amplitude numerical oscillations in the pressure field (of order 5×10^{-3}); these oscillations are practically negligible for larger times, due to the range of pressures developed.**

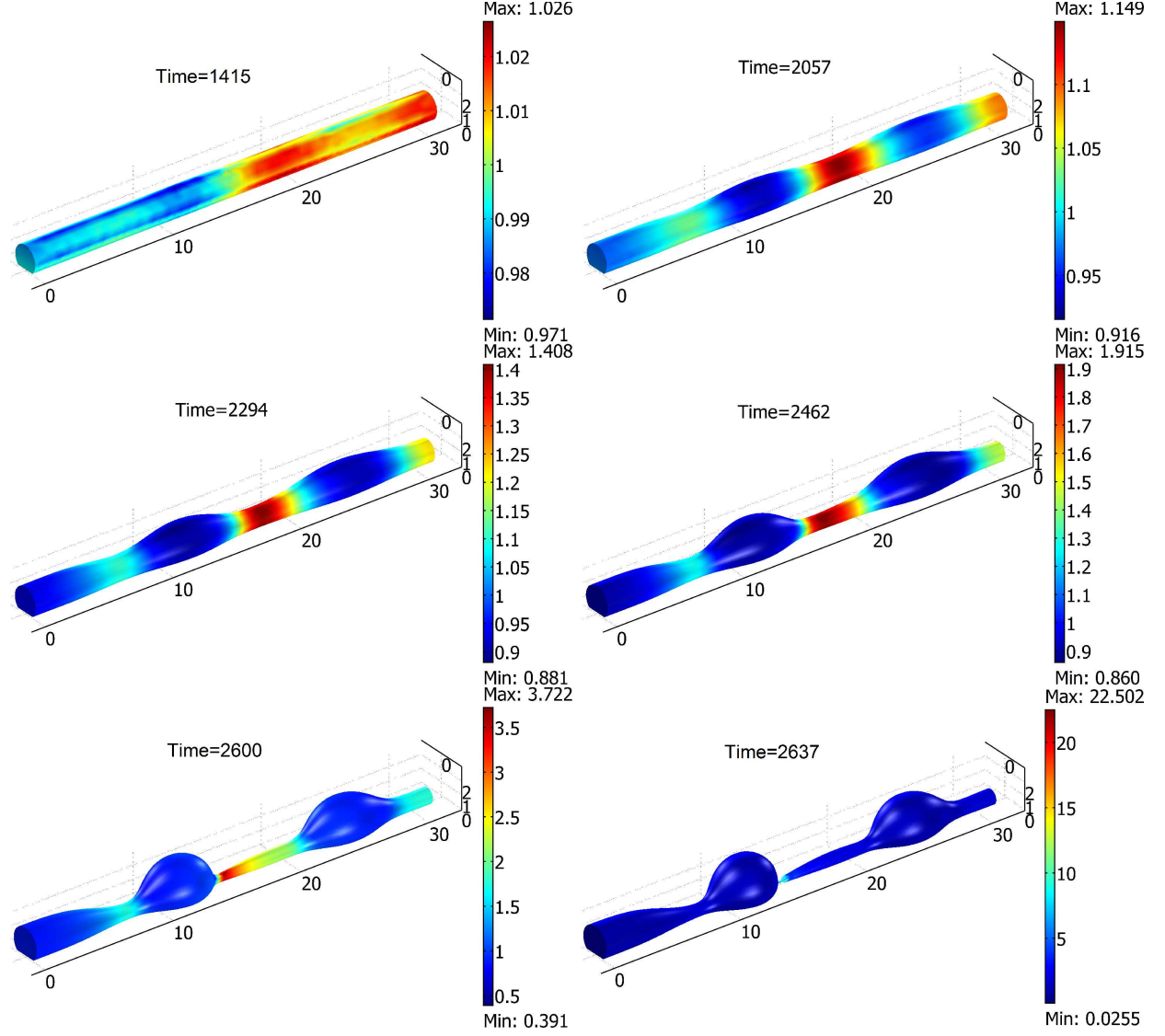


FIG. 11. (Colour online) The time evolution of a liquid strip with an initial perturbation of wave number $\hat{k} = 0.1$. The remaining parameters are $\theta = 3\pi/4$ ($\hat{A} = 2.86$), $Bo\hat{A} = 0.012$ and $La\hat{A}^{1/2} = 1.24 \times 10^4$. Shadings (colours in online version) indicate values of pressure (scale on the right of each frame). Instants of dimensionless time are printed for reference. The corresponding dimensional times (considering $R = 1.46 \times 10^{-4}$ m, $\sigma = 0.05$ N m $^{-1}$ and $\mu = 0.001$ Pa s) are 4.14×10^{-3} s, 6.02×10^{-3} s, 6.72×10^{-3} s, 7.21×10^{-3} s, 7.61×10^{-3} s and 7.72×10^{-3} s. **The noisy variations in shading (colour in online version) visible for $t = 1415$ are partly due to a lightning effect in the picture and partly due to small amplitude numerical oscillations in the pressure field (of order 5×10^{-3}); these oscillations are practically negligible for larger times, due to the range of pressures developed.**

of the strip. This allows us to study the time evolution of individual spatial modes and obtain the dispersion relationship of the system. We also analysed the late development of the instability, for liquid filaments several times longer than the computed fastest growing wavelength, until practically a first breakup of the thread is attained.

In real fluid strips, the finite size or any eventual geometric constraints will limit the selection of modes. Intuition indicates that the line of fluid will tend to break up according to the fastest growing spatial mode (among those permitted). Our computations suggest that this reasoning gives in general a very good estimate of the number of the main (in terms of size) resulting droplets, independently of the contact angle or viscosity of the fluid. However, the precise rupture pattern (having droplets both large and small interspersed at varying distances) does seem to depend on these parameters.

One also expects that growth rates give an indication of the time scale of the break up process. According to our results, this is indeed the case when one compares the rupture times of section IV B 2 with the growth rates computed in section IV B 1. For contact angles up to $\pi/2$, lubrication-based theories like those of Yang and Homsy¹⁵ and Diez, González, and Kondic¹² give an excellent prediction of the critical wave number. Besides, for moderate contact angles (see Fig. 5, corresponding to $\theta = \pi/6$) they also provide a very good estimate of growth rates. Our numerical results including inertia indicate that in this case α , the dimensionless growth rate, could be overestimated by roughly 20% when inertia is ignored. However, for larger contact angles (see Fig. 6 for $\theta = \pi/2$ and Fig. 7 for $\theta = 3\pi/4$), growth rates could be overestimated by one order of magnitude when inertia should be important and yet is neglected. This affects considerably the time of rupture of the rivulet (see Figs. 8–11) and could have important implications for practical applications. Note however that if, as in our case, the increase of the relative importance of inertia is achieved by diminishing the viscosity of the liquid, the dimensional growth rates of less viscous fluids are still larger than these of more viscous liquids, though not so large as a theory that ignores inertia would have predicted.

On the other hand, inertia seems to have only a weak influence on the wave number of the fastest-growing mode, according to the results of Figs. 5–7. In general terms, \hat{k}_M increases slightly as La augments.

Our results also suggest that for large contact angles (non-wetting case) the number of satellite droplets that tend to form is larger than for small contact angles (wetting case), at

least for viscous liquid filaments. This result is in qualitative agreement with the experiments of González *et al.*¹⁸, who observed a large number of satellite droplets in the rupture of viscous strips under partially wetting conditions. Due to limitations in our numerical scheme (simulations stop when the first pinch-off is attained), we can not ascertain to the validity of this statement for less viscous liquid rivulets.

This is a first study of the influence of inertia on the stability of deposited fluid filaments. Future work will complement this investigation and address other topics such as the influence of gravity when contact angles are large, the influence of more complex behaviours of the contact line, and finite size effects.

ACKNOWLEDGMENTS

We acknowledge financial support from CONICET, ANPCyT and UNL. Part of this work also was carried out while Paul Grassia was a Royal Academy of Engineering/Leverhulme Trust Senior Research Fellow and funding from the fellowship is gratefully acknowledged.

REFERENCES

- ¹A. Piqué and D. B. Chrisey, *Direct-write technologies for rapid prototyping applications: sensors, electronics, and integrated power sources* (Academic Press, San Diego, 2002).
- ²P. Calvert, “Inkjet printing for materials and devices,” *Chemistry of Materials* **13**, 3299–3305 (2001).
- ³J. A. Lewis and G. M. Gratson, “Direct writing in three dimensions,” *Materials Today* **7**, 32–39 (2004).
- ⁴J. A. Lewis, “Direct ink writing of 3d functional materials,” *Advanced Functional Materials* **16**, 2193–2204 (2006).
- ⁵P. Duineveld, M. de Kok, M. Buechel, A. Sempel, K. Mutsaers, P. van de Weijer, I. Camps, T. van de Biggelaar, J. Rubingh, and E. Haskal, “Ink-jet printing of polymer light-emitting devices,” in *Proceedings of SPIE*, Vol. 4464 (2002) pp. 59–67.
- ⁶L. Kondic, J. Diez, P. Rack, Y. Guan, and J. Fowlkes, “Nanoparticle assembly via the dewetting of patterned thin metal lines: Understanding the instability mechanisms,” *Physical Review E* **79**, 026302 (2009).

- ⁷A. Darhuber and S. Troian, “Principles of microfluidic actuation by modulation of surface stresses,” *Annual Review of Fluid Mechanics* **37**, 425–455 (2005).
- ⁸S. Davis, “Moving contact lines and rivulet instabilities. Part 1. The static rivulet,” *Journal of Fluid Mechanics* **98**, 225–242 (1980).
- ⁹G. Young and S. Davis, “Rivulet instabilities,” *Journal of Fluid Mechanics* **176**, 1–31 (1987).
- ¹⁰S. Mechkov, M. Rauscher, and S. Dietrich, “Stability of liquid ridges on chemical micro- and nanostripes,” *Physical Review E* **77**, 061605 (2008).
- ¹¹K. Sekimoto, R. Oguma, and K. Kawasaki, “Morphological stability analysis of partial wetting,” *Annals of Physics* **176**, 359–392 (1987).
- ¹²J. Diez, A. González, and L. Kondic, “On the breakup of fluid rivulets,” *Physics of Fluids* **21**, 082105 (2009).
- ¹³D. Langbein, “The shape and stability of liquid menisci at solid edges,” *Journal of Fluid Mechanics* **213**, 251–265 (1990).
- ¹⁴R. Roy and L. Schwartz, “On the stability of liquid ridges,” *Journal of Fluid Mechanics* **391**, 293–318 (1999).
- ¹⁵L. Yang and G. Homsy, “Capillary instabilities of liquid films inside a wedge,” *Physics of Fluids* **19**, 044101 (2007).
- ¹⁶S. Schiaffino and A. Sonin, “Formation and stability of liquid and molten beads on a solid surface,” *Journal of Fluid Mechanics* **343**, 95–110 (1997).
- ¹⁷P. Duineveld, “The stability of ink-jet printed lines of liquid with zero receding contact angle on a homogeneous substrate,” *Journal of Fluid Mechanics* **477**, 175–200 (2003).
- ¹⁸A. González, J. Diez, R. Gratton, and J. Gomba, “Rupture of a fluid strip under partial wetting conditions,” *EPL (Europhysics Letters)* **77**, 44001 (2007).
- ¹⁹C. Huh and L. Scriven, “Hydrodynamic model of steady movement of a solid/liquid/fluid contact line,” *Journal of Colloid and Interface Science* **35**, 85–101 (1971).
- ²⁰J. Donea, A. Huerta, J.-P. Ponthot, and A. Rodríguez-Ferran, “Arbitrary Lagrangian-Eulerian methods,” in *Encyclopedia of Computational Mechanics*, edited by E. Stein, R. de Borst, and T. Hughes (John Wiley & Sons, Ltd, 2004) pp. 243–299.
- ²¹H. Lamb, *Hydrodynamics* (Dover Publications, 1932), arts. 327 and 331.
- ²²C. Hirt and B. Nichols, “Volume of fluid (VOF) method for the dynamics of free boundaries,” *Journal of Computational Physics* **39**, 201–225 (1981).

- ²³D. Gueyffier, J. Li, A. Nadim, R. Scardovelli, and S. Zaleski, “Volume-of-fluid interface tracking with smoothed surface stress methods for three-dimensional flows,” *Journal of Computational Physics* **152**, 423–456 (1999).
- ²⁴M. Sussman, P. Smereka, and S. Osher, “A level set approach for computing solutions to incompressible two-phase flow,” *Journal of Computational Physics* **114**, 146–146 (1994).
- ²⁵J. Sethian, “Level set methods for fluid interfaces,” *Annual Review of Fluid Mechanics* **35**, 341–372 (2003).
- ²⁶G. Caginalp, “An analysis of a phase field model of a free boundary,” *Archive for Rational Mechanics and Analysis* **92**, 205–245 (1986).
- ²⁷D. Anderson, G. McFadden, and A. Wheeler, “Diffuse-interface methods in fluid mechanics,” *Annual Review of Fluid Mechanics* **30**, 139–165 (1998).
- ²⁸J. Donea, P. Fasoli-Stella, and S. Giuliani, “Finite element solution of transient fluid-structure problems in Lagrangian coordinates,” in *Proceedings of the International Meeting on Fast Reactor Safety and Related Physics, Chicago*, Vol. 3 (1976) pp. 1427–1435.
- ²⁹J. Fukai, Z. Zhao, D. Poulikakos, C. Megaridis, and O. Miyatake, “Modeling of the deformation of a liquid droplet impinging upon a flat surface,” *Physics of Fluids A: Fluid Dynamics* **5**, 2588–2599 (1993).
- ³⁰T. Hughes, W. Liu, and T. Zimmermann, “Lagrangian-Eulerian finite element formulation for incompressible viscous flows,” *Computer Methods in Applied Mechanics and Engineering* **29**, 329–349 (1981).
- ³¹J. Donea, S. Giuliani, and J. Halleux, “An arbitrary Lagrangian-Eulerian finite element method for transient dynamic fluid-structure interactions,” *Computer Methods in Applied Mechanics and Engineering* **33**, 689–723 (1982).
- ³²K. Christodoulou and L. Scriven, “Discretization of free surface flows and other moving boundary problems,” *Journal of Computational Physics* **99**, 39–55 (1992).
- ³³C. Hirt, A. Amsden, and J. Cook, “An arbitrary Lagrangian-Eulerian computing method for all flow speeds,” *Journal of Computational Physics* **135**, 203–216 (1997).
- ³⁴COMSOL AB, *COMSOL Multiphysics modeling guide. Version 3.5* (COMSOL, 2008).
- ³⁵A. Winslow, “Numerical solution of the quasilinear poisson equation in a nonuniform triangle mesh,” *Journal of Computational Physics* **1**, 149–172 (1966).
- ³⁶O. Zienkiewicz, R. Taylor, and J. Zhu, *The finite element method (6th edition): Volume 1 - Its basis and fundamentals* (Butterworth-Heinemann, 2005).

³⁷S. Ubal, B. Xu, P. Grassia, and B. Derby, “Continuous deposition of a liquid thread onto a moving substrate. numerical analysis and comparison with experiments,” *Journal of Fluids Engineering* **134**, 021301–17 (2012).

³⁸F. Brochard-Wyart and C. Redon, “Dynamics of liquid rim instabilities,” *Langmuir* **8**, 2324–2329 (1992).

³⁹This should be contrasted with the smaller contact angle predictions discussed previously (11 large droplets and 3 smaller droplets) so larger contact angles seems to favour the production of small satellites. *Note that satellite droplets have been observed experimentally, for example in González *et al.*¹⁸.*